Biochemistry

 Volume 40, Number 4 January 30, 2001

Accelerated Publications

Transition State Structure of Purine Nucleoside Phosphorylase and Principles of Atomic Motion in Enzymatic Catalysis[†,‡]

A. Fedorov,[§] W. Shi,[§] G. Kicska,[§] E. Fedorov,[§] P. C. Tyler,[||] R. H. Furneaux,[||] J. C. Hanson,[⊥] G. J. Gainsford,[||] J. Z. Larese,[⊥] V. L. Schramm,*[,§] and S. C. Almo[§]

Department of Biochemistry, Albert Einstein College of Medicine, 1300 Morris Park Avenue, Bronx, New York 10461, Industrial Research Limited, Lower Hutt, New Zealand, and Brookhaven National Laboratory, Upton, New York 11973

Received October 30, 2000; Revised Manuscript Received November 30, 2000

ABSTRACT: Immucillin-H [ImmH; (1*S*)-1-(9-deazahypoxanthin-9-yl)-1,4-dideoxy-1,4-imino-D-ribitol] is a 23 pM inhibitor of bovine purine nucleoside phosphorylase (PNP) specifically designed as a transition state mimic [Miles, R. W., Tyler, P. C., Furneaux, R. H., Bagdassarian, C. K., and Schramm, V. L. (1998) *Biochemistry 37*, 8615−8621]. Cocrystals of PNP and the inhibitor are used to provide structural information for each step through the reaction coordinate of PNP. The X-ray crystal structure of free ImmH was solved at 0.9 Å resolution, and a complex of PNP·ImmH·PO_4 was solved at 1.5 Å resolution. These structures are compared to previously reported complexes of PNP with substrate and product analogues in the catalytic sites and with the experimentally determined transition state structure. Upon binding, ImmH is distorted to a conformation favoring ribosyl oxocarbenium ion formation. Ribosyl destabilization and transition state stabilization of the ribosyl oxocarbenium ion occur from neighboring group interactions with the phosphate anion and the 5′-hydroxyl of the ribosyl group. Leaving group activation of hypoxanthine involves hydrogen bonds to O6, N1, and N7 of the purine ring. Ordered water molecules provide a proton transfer bridge to O6 and N7 and permit reversible formation of these hydrogen bonds. Contacts between PNP and catalytic site ligands are shorter in the transition state analogue complex of PNP·ImmH·PO_4 than in the Michaelis complexes of PNP·inosine·SO_4 or PNP·hypoxanthine·ribose 1-PO_4. Reaction coordinate motion is dominated by translation of the carbon 1′ of ribose between relatively fixed phosphate and purine groups. Purine and pyrimidine phosphoribosyltransferases and nucleoside *N*-ribosyl hydrolases appear to operate by a similar mechanism.

Kinetic isotope effect analyses of *N*-ribosyltransferase reactions have established ribosyl oxocarbenium ion character as a universal feature of their transition states (*1*−*3*). However, crystal structures of *N*-ribosyltransferases reveal a surprising lack of catalytic site features evolved to stabilize

[†] This research was supported by the National Institutes of Health (V.L.S. and S.C.A.) and the New Zealand Foundation for Research, Science, and Technology (R.H.F.). Beamlines X9B and X7B at the Brookhaven National Laboratory are supported by Facility Resource Grants RR01633 from the NIH and DE-AC02-CH100886 from the DOE.

[‡] The coordinates for bovine PNP·ImmH·PO_4 have been deposited with the Protein Data Bank (ID code 1B8O). Coordinates for immucillin-H·HCl have been deposited with the Cambridge Crystallographic Data Centre (deposition number CCDC 153632).

* Address correspondence to this author: tel, (718) 430-2813; fax, (718) 430-8565; e-mail, vern@aecom.yu.edu.

[§] Albert Einstein College of Medicine.

[||] Industrial Research Limited.

[⊥] Brookhaven National Laboratory.

10.1021/bi002499f CCC: $20.00
Published on Web 12/30/2000

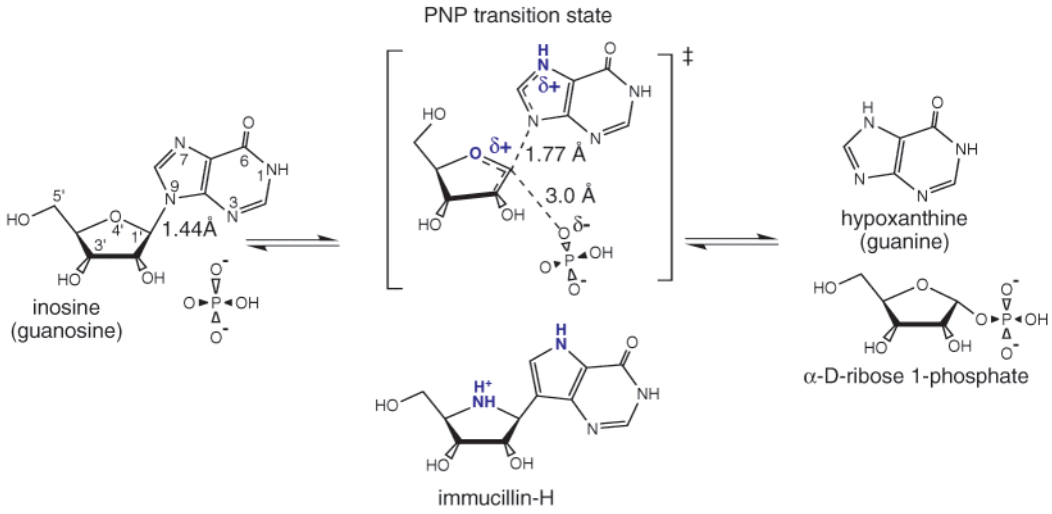

FIGURE 1: PNP-catalyzed phosphorolysis of purine nucleosides: transition state and transition state analogue inhibitor immucillin-H. The stabilized oxocarbenium ion nature of the transition state is derived from the analysis of kinetic isotope effects (*1*, *15*). Bond lengths to the hypoxanthine leaving group and to the phosphate nucleophile are compared for inosine and the transition state. Immucillin-H is a transition state inhibitor and is compared with inosine in the transition state complex. The protonated iminoribitol ring of ImmH resembles the positively charged oxocarbenium ion in the transition state, and the chemically stable C9−C1′ bond replaces the labile N9−C1′ ribosidic bond. The pK_a of N7 is greater in ImmH[2] than in inosine, a change that also occurs in formation of the transition state. Both substitutions shown in blue are necessary for binding as a transition state analogue.

oxocarbenium transition states (*4*−*6*). In contrast, the catalytic sites of glucosyl hydrolases have highly conserved pairs of carboxylates that sandwich and stabilize glucose oxocarbenium transition states (*7*, *8*). The crystal structure of bovine purine nucleoside phosphorylase (PNP) with immucillin-H (ImmH,[1] a transition state inhibitor) is reported here and is compared with the experimentally determined transition state and with structures of PNP complexes with reactants and with products. The analysis reveals unprecedented detail of the transition state and catalytic site motion. The enzyme distorts the substrate to favor electronic interactions for transition state formation. Enzyme-induced neighboring group electrostatic interactions and leaving group activation generate the transition state. The PNP complex with ImmH is closely related to the actual transition state previously established by kinetic isotope effects. We find that the reaction coordinates for PNP and other *N*-ribosyltransferases are dominated by nonclassical atomic motion (*9*, *10*) of ribose between two enzymatically constrained nucleophiles, resulting in nucleophilic displacements by electrophile migration.

Mammalian PNP catalyzes the reversible phosphorolysis of hypoxanthine or guanine ribonucleosides and 2′-deoxyribonucleosides to the free purine bases and the corresponding α-D-ribosyl 1-phosphates (Figure 1; *11*, *12*). Genetic deficiency of PNP causes T-cell immunodeficiency due to the toxic accumulation of dGTP, while B-cells and other tissues are largely unaffected (*13*). Autoimmune disorders, tissue transplant rejection, and several cancers are T-cell mediated and, therefore, make PNP a significant target for inhibitor design. Here we describe the 0.9 Å resolution structure of ImmH, a transition state analogue inhibitor for PNP and the 1.5 Å resolution crystal structure of bovine PNP complexed with ImmH and inorganic phosphate (Figure 2). Comparison of these structures to PNP complexes with substrates, products, and the experimentally determined transition state structure provides unprecedented atomic resolution along the reaction coordinate of this important enzyme (Figure 3).

METHODS

Structural Methods for ImmH. Immucillin-H, hydrochloride salt, was crystallized as a stack of thin plates. Diffraction data were collected at the Brookhaven National Laboratory, Synchrotron Light Source beamline X7B. The incident wavelength was 0.9370 Å. Three data sets were collected with a MAR345 image plate detector and integrated using the HKL suite of programs (*29*). The structure was solved by direct methods and refined with the Brucker shelxtl suite of programs. There were 9965 observations that were merged with 2/*m* symmetry to give an $R_{merge} = 0.067$. The R1 for 637 data is 0.109 (0.097 on 586 data, $F > 4\sigma$) and wR2 = 0.270 and the data extended to 0.95 Å ($R_{merge} = \sum(I - \langle I \rangle)^2/\sum I^2$, $R1 = \sum||F_o| - |F_c||/\sum|F_o|$, $wR2 = [\sum[w(F_o^2 - F_c^2)]^2/\sum[wF_o^2]^2]^{1/2}$). Bond distances were restrained to that of related structures with a σ of 0.03 Å.

Crystallization, Data Collection, Processing, and Refinement of PNP. Calf spleen PNP was purchased from Sigma and purified by affinity chromatography on modified Sepharose (*30*). Solutions of 30 mg/mL PNP in 10 mM phosphate buffer were incubated with a 1:1.1 molar excess of inhibitor for 2 h. Crystals were grown by hanging drop vapor diffusion after mixing equal volumes of enzyme and a reservoir solution containing 35% PEG 400, 100 mM Tris buffer, pH 8.0, 100 mM $MgCl_2$, and 10 mM potassium phosphate. X-ray diffraction data were collected at −178 °C on a MAR345 image plate using synchrotron radiation from beamline X9B at the National Synchrotron Light Source, Brookhaven National Laboratory. Data were processed using HKL (*29*). Diffraction was consistent with the cubic space group $P2_13$ ($a = 92.68$ Å) with one monomer per asymmetric unit. The data used in the structure determination and

[1] Abbreviations: ImmH, immucillin-H, (1*S*)-1-(9-deazahypoxanthin-9-yl)-1,4-dideoxy-1,4-imino-D-ribitol); PNP, purine nucleoside phosphorylase; K_i*, dissociation constant for a slow-onset tight binding inhibitor that includes the slow-onset, slow-release components (see ref *14*); PDB, Protein Data Bank; PEG, poly(ethylene glycol).

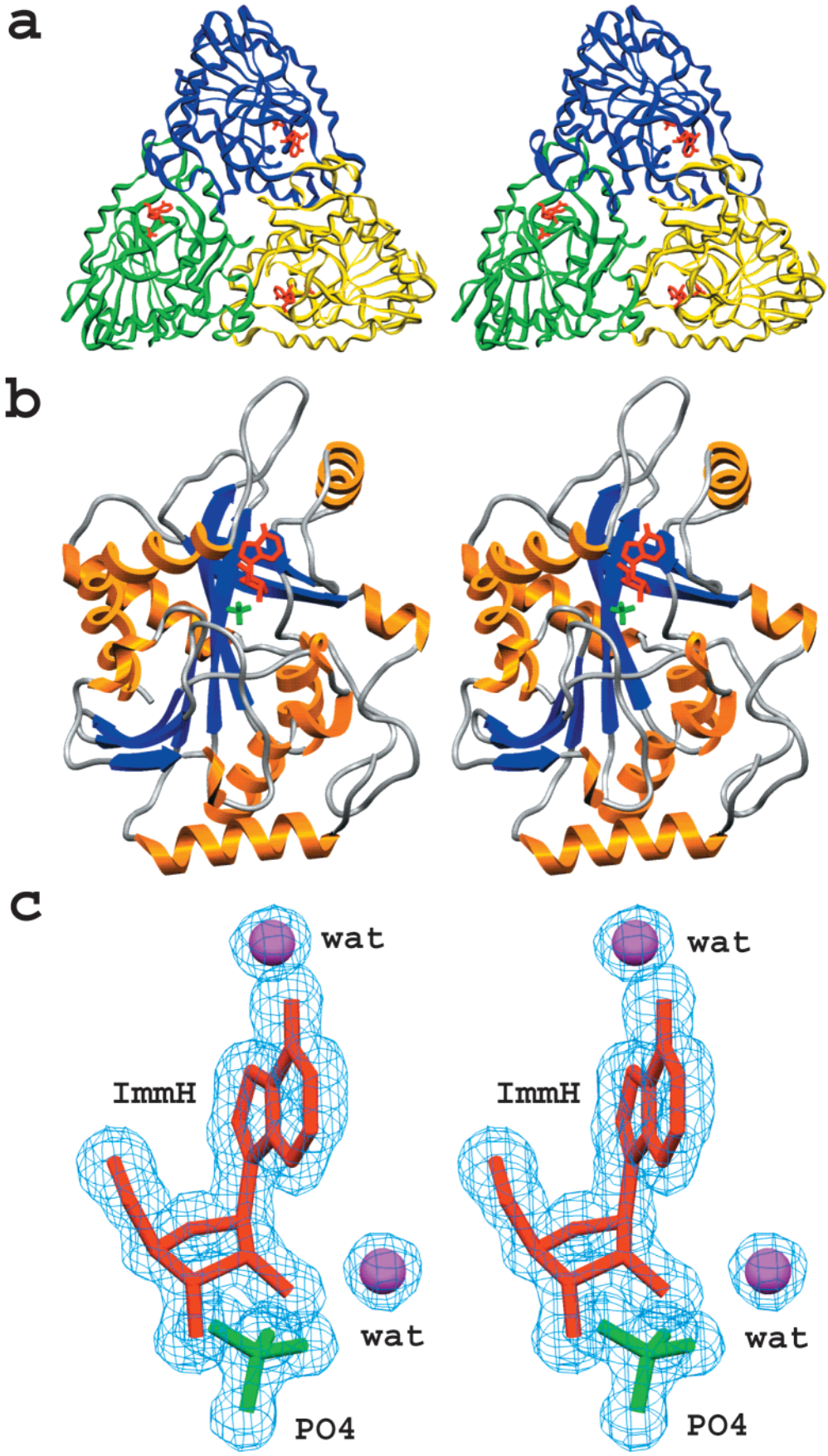

FIGURE 2: Stereo diagrams of bovine PNP trimer (a), monomer (b), and bound ImmH and phosphate (c). The relatively open appearance of the catalytic site in the monomer is altered by the participation of a loop from the neighboring subunit (compare panels a and b). The stereoview of the $2F_o - F_c$ electron density map for bound ImmH and PO_4 is contoured at 1σ (c). The inhibitor is shown in red, phosphate ion is shown in green, and two catalytic site water molecules are shown in purple. At this stage of the refinement all ligands and solvent molecules were not yet included in the model. The figures were generated using SETOR (*34*).

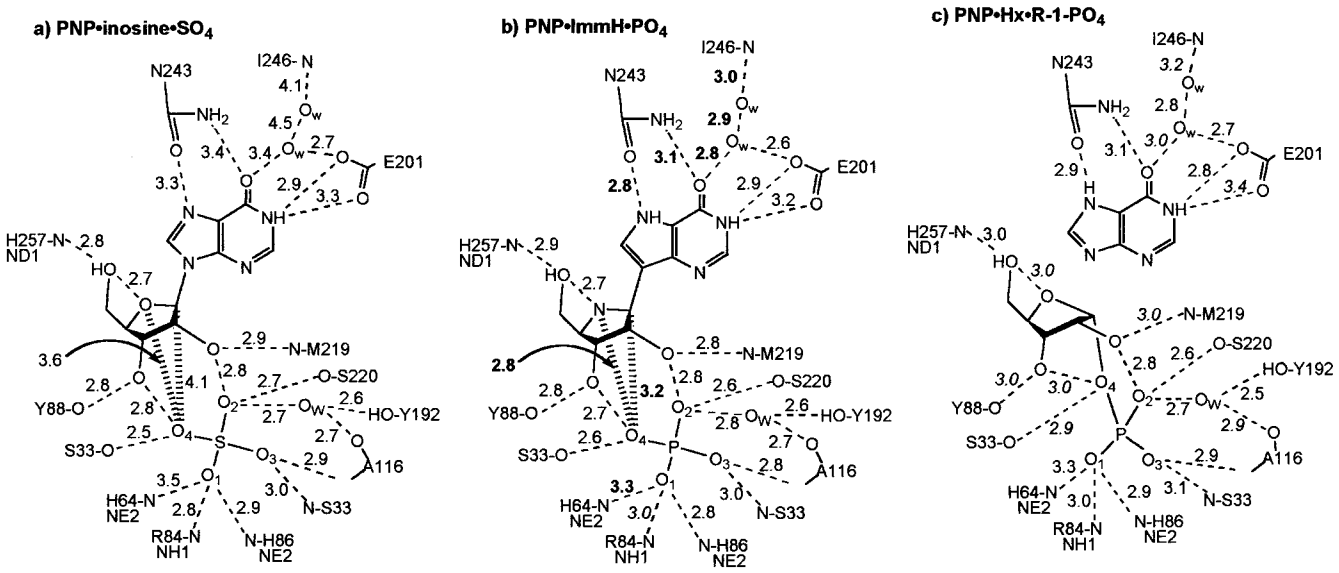

FIGURE 3: Noncovalent interactions in the active sites of bovine PNP complexes. Contacts ≤3.3 Å in the PNP•ImmH•PO_4 complex (b) [PDB 1B8O (this work)] are compared with those of PNP•inosine•SO_4 (a) [PDB 1A9S (*17*), a Michaelis complex] and with those of PNP•hypoxanthine•ribose 1-PO_4 (c) [PDB 1A9T (*17*), the product complex]. Distances are indicated in angstroms. In (b), atomic distances that are 0.2 Å shorter than in (a) are shown in bold, and those that are at least 0.2 Å or more longer in (b) than (a) are shown in italics. In (c), atomic distances that are at least 0.2 Å longer in (c) than in (b) are in italics.

refinement were 92.6% complete at 2σ(*F*) cutoff to 1.5 Å with an R_{merge} of 6.0%. The PNP complex with ImmH was solved by molecular replacement with X-PLOR (*31*), using native calf spleen PNP (PDB file 1PBN) as the search model (*12*). Rotation and translation searches gave the expected solutions with the PNP trimer lying along the 3-fold crystallographic axis. Rigid body refinement yielded an initial *R*-factor of 34% in the resolution range 15−4 Å. One cycle of simulated annealing refinement resulted in the clear identification of inhibitor and phosphate ion. Further refinement was performed with manual refitting after each cycle. Loops containing amino acids 33−36, 56−69, and 241−266 were substantially rebuilt. The free *R*-factor (*32*) was used for cross validation throughout the refinement. Water molecules (200) were added for density peaks >4σ in difference maps when appropriately hydrogen bonded. The model displayed good stereochemistry for the amino acids as determined by PROCHECK (*33*), with 93.6% in the most favored region, 5.9% in additionally allowed regions, and Thr221 in the disallowed region, but revealing clear electron density in omit maps.

Table 1: Data Collection and Refinement Statistics

Data Collection	
resolution range, Å	20.0−1.5
unique reflections	42526
completeness, % [at 0σ(*I*) cutoff]	99.6
R_{merge}, %	6.0
mean $I/\sigma(I)$	40.0
wavelength, Å	1.04019
Refinement Statistics	
resolution used, Å	8.0−1.5
reflection used (92.6% complete, 2σ cutoff)	39199
R_{cryst}, %	18.4
R_{free}, %	23.2
RMS Deviations	
bond, Å	0.007
angle, deg	1.3
dihedrals, deg	25.4
improper, deg	0.75
Average *B* Factor, Å^2	
overall	17.4
protein	15.8
water	19.2
ligands	12.7

RESULTS AND DISCUSSION

Properties of ImmH. Immucillin-H is a transition state inhibitor of PNP (K_i* = 23 pM), designed and synthesized specifically to mimic the transition state structure (Figure 1; *14*−*16*). The 4′-imino group replaces the O4′ ribosyl oxygen of inosine and, on protonation,[2] mimics the partial positive charge of the ribooxocarbenium transition state. Chemical stability of ImmH is provided by the C−C ribosidic bond. The deazahypoxanthine ring of ImmH is protonated at N7 (pK_a = 9.8) similar to inosine at the transition state and unlike N7 in the substrate (pK_a = 1.2) (Figure 1). These electronic features cause ImmH to bind 1 million times tighter to PNP than the substrate inosine (*14*). The X-ray crystal structure of the hydrochloride form of ImmH was solved and is discussed below in comparison with enzyme-bound Imm-H.

Structure of PNP•ImmH•PO_4 at 1.5 Å Resolution. Crystals of bovine PNP•ImmH•PO_4 were prepared by hanging drop vapor diffusion, and data were collected to 1.5 Å (Table 1). The structure of the ternary PNP•ImmH•PO_4 complex resembles the structures of PNP•inosine•SO_4 (reactants) and

[2] The ionic state of bound ImmH in complexes with PNP has not been established. Titrations of ImmH with acid/base cycles and proton NMR analyses have established pK_a values of 9.8 for ionization of the N7 to form the monoanion, 6.5 for formation of the N4′ iminoribitol monocation, and 1.5 for formation of the N3, N4′ dication (A. A. Sauve and V. L. Schramm, unpublished observations).

PNP·hypoxanthine·ribose 1-PO_4 (products), but the PNP·ImmH·PO_4 complex involves closer contacts between the protein and ImmH (Figure 2 and 3; *17*). The molecular 3-fold axis of PNP is coincident with the crystallographic 3-fold axis in cubic space group $P2_13$, enforcing a fully symmetric homotrimer. Subunits of PNP are constructed around a core composed of an eight-stranded β-sheet and a smaller five-stranded β-sheet, surrounded by nine α-helices and two short 3/10-helices. Each active site of PNP resides in a deep cavity near the interface with a neighboring subunit (Figure 2a,b). Two catalytic site loops change conformation upon phosphate binding, while a third loop changes its conformation upon binding of nucleoside substrates, purine products, or the inhibitor ImmH (*17*). The high-temperature factors reported for the purine-dependent loop in native PNP decrease upon ligand binding and are accompanied by the transition to a short α-helix. Electron density ($F_o - F_c$ and $2F_o - F_c$) of bound ImmH and phosphate places the phosphate directly under the iminoribitol ring of the inhibitor with two nearby water molecules (Figure 2c). The PNP·ImmH·PO_4 complex is characterized by 40 catalytic site contacts closer than 3.5 Å. The high affinity for ImmH correlates with eight interactions that shorten in the complex (Figure 3a,b) and with decreased protein dynamics as measured by slowed solvent exchange in the peptide backbone (*18*). In particular, the Michaelis and product complexes of PNP·inosine·SO_4 and PNP·hypoxanthine·ribose 1-PO_4 have reaction coordinate distances (from N9 of inosine or hypoxanthine to O4 of the phosphate group) of 5.6 and 5.2 Å, respectively, which shorten to 4.8 Å in the transition state analogue complex of PNP·ImmH·PO_4. This distance is mechanistically significant, since approximately 6 Å is required for formation of a fully developed S_N1 transition state, while shorter distances dictate transition state formation with significant bond order to leaving and/or attacking groups (see below).[3]

Phosphate Interactions. Formation of the transition state in PNP generates a highly reactive C1′ that migrates to react with phosphate O4. The 10 relatively well-positioned H-bonds to the phosphate oxygens render the anion nearly immobile at the catalytic site, making O4 the most accessible and nucleophilic anionic oxygen of bound phosphate (Figure 3b). Protein contacts to PO_4 in the PNP·ImmH·PO_4 complex include a single relaxed interaction, that with Arg84, to increase its nucleophilic character. Favorable hydrogen bonds (2.8 Å) between two phosphate oxygens and the 2′- and 3′-hydroxyls of the iminoribitol align the ribosyl and phosphate groups and result in a major structural change in the glycosidic torsion angle of ImmH as it binds to the enzyme (Figure 4e,f).

PNP-Induced Distortion of ImmH. Comparison of free and bound ImmH geometry was made using the $2F_o - F_c$ electron density from PNP·ImmH·PO_4 and the small molecule crystal structure of immucillin-H·HCl. Binding of ImmH to PNP enforces a specific conformation of the inhibitor. The 5′-hydroxyl torsion angle (O5′−C5′−C4′−N4′) and the glycosidic torsion angle (N4′−C1′−C9−C8), respectively, change from +40° and −47°, seen in the small molecule crystal structure of immucillin-H·HCl (Figure 4f), to −66° and +66° for ImmH in the PNP·ImmH·PO_4 complex (Figure 4e). Similarly, the conformation of the iminoribitol moiety changes from a C2′-endo to a C4′-endo on formation of the complex. The enzyme-bound conformation is energetically unfavorable for purine nucleosides and differs from other nucleotides and nucleosides bound to proteins (*19*). Formation of transition states with ribooxocarbenium ion character is most favored with orbital overlap between the breaking N9−C1′ bond and the C2′−H2′ bond of inosine (an N9−C1′−C2′−H2′ dihedral angle near 0°) (*1*, *20*). This angle is 42° in the small molecule ImmH structure. Binding of ImmH to PNP alters the C9−C1′−C2′−H2′ dihedral angle to 0°. Thus, PNP causes bound

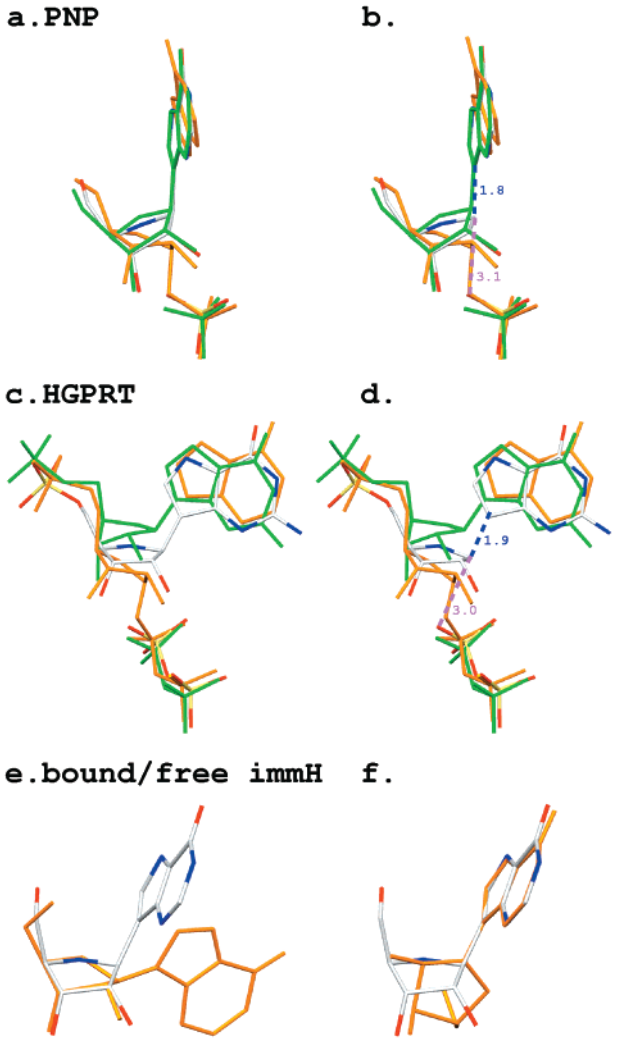

FIGURE 4: Superpositions of the reactants (green), bound transition state analogues (white with blue nitrogens and red oxygens), and products (gold) in the active sites of bovine PNP (a) and of purine phosphoribosyltransferases (HGPRT, c) are compared with the superpositions of reactants, experimentally determined transition states, and products (b) and (d). Distances (in angstroms) shown in (b) and (d**)** are deduced from transition state analyses for PNP and orotate phosphoribosyltransferase (*2*, *15*). PDB codes for (a) are 1A9S, 1B8O, and 1A9T, as in Figure 3. The reactant, transition state analogue, and product structures for HGPRT (c**)** are from 9-deazahypoxanthine and PRPP in *Trypanosoma cruzi* HPRTase (PDB 1TC2, in gold), immucillin-GP and PP_i in human HGPRTase (white with blue nitrogens and red oxygens, PDB 1BZY), and products XMP and PP_i in *Toxoplasma gondii* HGPRTase (in green, PDB 1QK5). Conformations of free and bound immucillins (e and f) are from the small molecule crystal structure of ImmH (gold) and ImmH in PNP·ImmH·PO_4 (PDB 1B8O, white with blue nitrogens and red oxygens). Molecular overlap in (e**)** is C3′ and C4′ and in (f**)** is the purine rings.

[3] We thank an anonymous reviewer for suggesting this comparison.

ImmH to adopt the optimal sugar pucker for O4′ stabilization of the oxocarbenium species (hyperconjugative transition state stabilization). Likewise, the 5′-hydroxyl is anti to the ribosyl group for purine nucleosides (*19*) but adopts an unfavorable syn configuration when bound to PNP, thus placing the 5′-oxygen within 2.7 Å of O4′ or N4′ (Figure 3a,b).

ImmH and the Transition State of PNP. The experimentally established transition state structure for phosphorolysis of inosine by PNP has been established from kinetic isotope effects (*15*) and is compared to the structure of bound ImmH (Figure 4a,b). The distance from C1′ to the O4 of the phosphate nucleophile is 3.2 Å in PNP·ImmH·PO_4 and is 3.0 Å in the experimentally determined transition state, values that are identical within the errors of the experimental methods (*15*). This distance is 4.1 Å in the Michaelis complex of PNP·inosine·SO_4, supporting ImmH as a close mimic of inosine at the transition state (Figure 3a,b). Eight contacts that stabilize the PNP·ImmH·PO_4 complex relative to PNP·inosine·SO_4 are indicated in Figure 3b. Several of these change from weak (>3.0 Å) to strong interactions (<2.8 Å) with bound ImmH. Short geometrically favorable hydrogen bonds are reported to have energies of activation of 7−8 kcal/mol in partial aqueous solvents (*21*); thus the improved hydrogen bonds surrounding ImmH can easily account for the 10^6-fold K_m/K_i* found for ImmH binding (*14*).

Transition State Formation. The transition state for phosphorolysis of inosine by PNP results from enzymatic forces that cause expulsion of electrons from the ribosyl ring and that generate an electron deficiency in the hypoxanthine leaving group. A 2.8 Å hydrogen bond between HN7 of bound ImmH and Asn243 OD1 is observed in the PNP·ImmH·PO_4 complex. An analogous interaction would stabilize a protonated N7 of inosine at the transition state. Atom O6 of ImmH accepts hydrogen bonds both from the NH_2 of Asn243 and from an enzyme-immobilized water molecule, and analogous interactions in the inosine complex cause electron withdrawal from the purine and favor heterolysis of the C1′−N9 bond. The distance between O6 and the neighbor water molecule decreases from 3.4 to 2.8 Å in PNP·inosine·SO_4 and PNP·ImmH·PO_4, respectively (Figure 3a,b). This water is in contact with a second ordered solvent molecule in a narrow channel, forming a proton transfer bridge to bulk water. This bridge is the source of the proton for the N7 hydrogen bond to the carboxamide oxygen of Asn243, since there is no enzymatic acid to donate this proton. Substantial electron withdrawal occurs through this hydrogen bond, since Asn243Ala retains only 0.1% of its catalytic activity (*22*). In addition, the substrate analogue 7-deazainosine binds well to PNP but is not a substrate (*12*). Carboxyl oxygens of Glu201 hydrogen-bond to the catalytic water and also accept a hydrogen bond from NH1 of the purine ring. The enzymatic interactions at N7 and especially at O6 of inosine generate an electron-deficient purine that withdraws electrons from the C1′ to N9 bond to favor N-ribosidic bond loss (electron pull). The O6 is an essential substrate feature; adenosine and adenine are not substrates. The unusual 5′-hydroxyl torsion angle places O5′ 2.7 Å above N4′, with O4 of phosphate 2.8 Å below the oxocarbenium oxygen. Sandwiching the ribosyl ring oxygen (O4′) of the nucleoside substrate between two electron-rich oxygens favors release of electrons from O4′, cleavage of the C1′−N9 bond, and formation of the ribooxocarbenium ion transition state (electron push). The 9-deazahypoxanthine and phosphate groups as well as the 5′-, 4′-, and 3′-carbons of the ribose ring are relatively fixed through the reaction (Figure 4a). The atomic positions reveal that the excursion from substrate to product is dominated by C1′-ribooxocarbenium motion, since N9, C1′, and phosphate O4 atoms move 0.7, 1.7, and 0.8 Å, respectively (Table 2).

Table 2: Atomic Excursions in the Reactions of PNP and HGPRT[a]

	PNP			HGPRT		
PNP complexes	N(C)9	C1′	O_4P(S)	N(C)9	C1′	O_4P
Ino·SO_4 → TS[b]	0.3	0.4	0.6	0.7	1.2	0.5
ImmH·PO_4 → TS	0.0	0.2	0.0	0.0	0.3	0.0
TS → Hx·R1PO_4[b]	0.8	1.3	0.4	1.1	1.1	0.8
Ino·SO_4 → Hx·R1PO_4	0.7	1.7	0.8	0.8	2.1	0.9

[a] Distances are linear interatomic distance changes in angstroms. All catalytic site ligands are referenced to adjacent atoms of the peptide backbone atoms that remain constant in all crystallographic structures described in the table. The direction of each atomic excursion is indicated in Figure 4. [b] The transition state (TS) bond lengths were taken from Kline and Schramm (*15*) for PNP and from Tao et al. (*2*) for HGPRT. Ino·SO_4, ImmH·PO_4, and Hx·R1PO_4 refer to the complexes with PNP. Ino, Hx, and R1PO_4 are inosine, hypoxanthine, and α-D-ribose 1-PO_4, respectively. This analysis assumes that transition state structures are similar for orotate and purine phosphoribosyltransferases (see ref *1*).

Furanose and pyranose sugars are prone to oxocarbenium ion formation (*9*); thus, it is of interest to compare the PNP transition state to a fully developed S_N1 transition state in which the reaction center is "exploded".[3] The transition state for PNP is reached when the N-ribosidic bond of inosine elongates from 1.44 to 1.77 Å and has lost approximately 65% of its covalent character (Pauling bond order) but before significant bond order is formed to the phosphate nucleophile (*15*). A fully developed S_N1 transition state with <0.01 bond order to either leaving group or attacking nucleophile at the transition state would require an additional 1.3 Å separation at N9−C1′ before the transition state is reached. The exploded transition state is unequivocally eliminated by kinetic isotope effect studies (*15*) and is further eliminated by the restricted reaction coordinate distance (phosphate to purine) imposed by the enzyme. The early transition state along a dissociative reaction coordinate path is further supported by the good agreement between the docked transition state and the geometry and tight binding of the ImmH complex (Figure 4b).

Reaction Coordinate Motion. The PNP-catalyzed phosphorolysis of nucleosides causes inversion of anomeric configuration at C1′. Nucleophilic displacements imply attack by the nucleophilic group, but here the phosphorus atom moves only 0.24 Å throughout the reaction coordinate (Figure 4a,b). Comparison of PNP·inosine·SO_4 to PNP·ImmH·PO_4 reveals a 15° tilt of the phosphate group that carries O4 of the phosphate 0.6 Å closer to the reaction center at C1′. This motion is not accompanied by similar changes in the PNP backbone or in amino acid side chains in contact with the phosphate. Thus the phosphate tilt is most likely caused by an electrostatic interaction between it and the N4′ of the iminoribitol ring, suggesting that the nitrogen is protonated to carry a positive charge, thus attracting the nearby phosphate oxygen and inducing the tilt. The peptide backbone

of Asn243 and side chain located above the purine ring move about 0.3 Å nearer ImmH, placing the inhibitor slightly deeper in the catalytic pocket than found with bound inosine (*17*). Combined, the phosphate tilt and the Asn243 loop motions bring the iminoribitol C1′ 0.9 Å nearer to O4 of phosphate in the complex of PNP·ImmH·PO_4 than in the PNP·inosine·SO_4 complex. The nucleophilic oxygen (O4 of phosphate, Figure 3b) is immobilized 2.8 Å from O3′ of iminoribitol and 2.6 Å to the hydroxyl of Ser33, fixing the position of O4 2.8 Å from N4′, the site of the O4′ oxocarbenium oxygen in the transition state. The N4′−O4 phosphate interaction in PNP·ImmH·PO_4 (2.8 Å) is considerably shorter than the O4′−O4 sulfate interaction in the PNP·inosine·SO_4 complex (3.6 Å), consistent with proposals for both substrate destabilization and transition state stabilization (Figure 3a,b). Attraction of bonding electrons from the N9−C1′ bond into the electron-deficient purine ring forms the ribooxocarbenium ion transition state. These interactions are weak in the structure of PNP·inosine·SO_4 (*17*, *23*) and only become energetically important at the transition state.

Oxocarbenium Ion Shielding. Sugar oxocarbenium ions are highly reactive to water, with an estimated lifetime of 10^{-12} s (*24*). Exclusion of mobile solvent water from the catalytic sites of *N*-ribosyltransferases is therefore critical to prevent hydrolysis. Hydrophobic residues Phe200, Met219, and Val245 from each subunit and Phe159 from the adjacent subunit partition the active sites from solvent. Despite the closed nature of the catalytic sites, two highly ordered water molecules are trapped in contact with the PNP·ImmH·PO_4 complex, but are partitioned from C1′, and a third forms a channel to solvent (Figures 2c and 3b).

Positions of Bound Intermediates. Atomic positions for reactants during the PNP-catalyzed phosphorolysis of inosine were proposed by superimposing segments of the peptide backbones near the catalytic sites that remain unchanged in the structures of the complexes of PNP with substrate, transition state analogue, and reaction products (Figure 4a,b). The O4′, C1′, and C2′ atoms of the ribose ring migrate away from the purine ring toward O4 of the phosphate group. Remarkably, there is only a single enzymatic contact relevant to ribosyl ring migration. This is the 2.8 Å hydrogen bond between the O2′ oxygen and the amide of Met219. The location of Met219 is invariant in PNP·inosine·SO_4, PNP·ImmH·PO_4, and PNP·hypoxanthine·ribose 1-PO_4 and serves as a fixed anchor point for reaction coordinate motion (Figure 3a,b). There are no enzymatic groups to directly stabilize the positive charge of a ribooxocarbenium ion transition state, although bound phosphate is well positioned for this role. Thus, formation of the transition state involves the electrostatically driven migration of the ribooxocarbenium carbon from the purine ring toward the phosphate. The transition state is reached when the C1′−N9 bond has lengthened by only 0.33 Å (Figure 1 and Table 2); however, substantial changes in the hydrogen bond distances to the protein accompany this change (compare a and b of Figure 3). Contact between C1′ and O4 of bound phosphate at this asymmetric transition state is limited to a van der Waals interaction of 3.0 Å. The point of atomic symmetry in the reaction coordinate of PNP occurs when C1′ translates an additional 0.6 Å past the transition state, giving partial bonds of 2.4 Å to both the purine and the phosphate. In terms of the chemical development of the reaction coordinate, this point is far past the transition state poise and is energetically similar to bound products.

Conformations for Product Release. Despite the structural changes that occur between the transition state and bound products (Figure 3c), interactions with the purine are similar in both complexes. As products form, the purine base and the catalytic site loop in contact with it (amino acids 242−247) move simultaneously in the same direction. Only the hydrogen bond between H_2O and atom O6 of the purine is weaker, increasing from 2.8 to 3.0 Å. These conserved interactions explain the unprecedented tight binding of hypoxanthine to PNP (1.3 pM) following the slow hydrolytic reaction of inosine to ribose and PNP·hypoxanthine and its rate-limiting release in the normal reaction of PNP (*25*).

Other Enzymes with Ribosyl Oxocarbenium Migration. The migrating oxocarbenium mechanism of PNP can also be recognized in other reactions involving *N*-ribosyl transfer, including the purine and pyrimidine phosphoribosyltransferases (Figure 4c,d) (*2*, *5*, *6*, *26*). These enzymes transfer ribose 5-phosphate between purine or pyrimidine bases and bound magnesium pyrophosphate. The pyrophosphate is immobilized by two bidentate magnesium ions in a scaffold of 12 noncovalent interactions (each 3.2 Å or less). The nucleophilic pyrophosphate oxygen and the purine N9 nitrogen atoms move 0.5 and 0.7 Å from the Michaelis complex to form the transition state (deduced from kinetic isotope effects on orotate phosphoribosyltransferase; *2*), while the C1′ of ribose undergoes a translational excursion of 1.2 Å (Figure 4c,d and Table 2). In the purine phosphoribosyltransferases, the C1′ excursion is 2.1 Å in converting bound substrates to bound products, while excursions of N9 and the phosphate oxygen nucleophile are less than half this distance at 0.8 and 0.9 Å, respectively. Recently, structural arguments have been used to support an S_N2 mechanism for phosphoribosyltransferases (*26*). However, reaction coordinate distances with bound transition state inhibitors (*5*, *6*) and kinetic isotope effects with orotate phosphoribosyltransferase (*2*) are compelling arguments for early transition states in dissociative mechanisms. The ultimate resolution of this debate awaits additional analyses by kinetic isotope effect studies.

A third enzymatic example of the ribooxocarbenium migration mechanism is provided by the nonspecific nucleoside *N*-ribosyl hydrolases. Like other *N*-ribosyltransferases the transition state also has ribooxocarbenium character (*20*). The purine *N*-ribosyltransferases feature an immobilized water nucleophile ligated to a catalytic site Ca^{2+} ion. No enzymatic groups are near the position corresponding to the ribosyl O4′ cation at the proposed transition state, based on the structure with a transition state analogue (*4*). By extension of the principles summarized here, nucleoside hydrolase is also proposed to catalyze its reaction by migration of the electrophile.

Defining Features of the Electrophile Migration Mechanism. Characteristics that are diagnostic for *N*-ribosyl transfer by electrophilic migration include the 4′-ribosyl ring oxygen sandwiched between a syn 5′-hydroxyl oxygen of ribose and a second oxygen under the ribose. This unusual interaction promotes loss of bonding electrons to the leaving group and formation of the highly reactive ribooxocarbenium transition state without requiring a direct contact from enzymatic

groups. Chemical evolution has distanced enzymatic groups from the highly reactive ribooxocarbenium ion and has placed the intended nucleophile (phosphate, water, or pyrophosphate) nearby for rapid capture of the ribosyl group. No enzymatic anions are sufficiently near C1′ or O4′ of ribose to permit ribooxocarbenium ion stabilization. Solvent water must be rigorously excluded from the ribooxocarbenium migration path to prevent hydrolysis in the phosphotransferases. Water molecules in complexes of PNP and purine phosphoribosyltransferases with bound transition state inhibitors demonstrate atomic rigidity similar to the peptide backbone and are carefully located out of the migration path. In the hydrolases the reactive water is immobilized by an 8-coordinate Ca^{2+} ion and placed directly in the migration path of the mobile ribooxocarbenium ion. Using these criteria, three groups of *N*-ribosyltransferase enzymes show evidence for nucleophilic displacement by electrophile migration in a minimal atomic motion reaction coordinate.

Retaining Ribosyl Transfer Mechanism. Similar to the catalytic mechanisms of glucosyltransferases, not all ribosyltransferases are characterized by concereted, inverting mechanisms. Many ribosyltransferases exhibit overall retention of anomeric configuration implicating chemical capture to form intermediates. NAD^+-dependent ADP-ribosyl cyclases and NAD^+ hydrolases form covalent intermediates, followed by hydrolysis or transfer to other acceptors with overall retention of configuration (*27*). Likewise, the deoxyribonucleoside transferases are known to form covalent deoxyribosyl intermediates (*28*). Kinetic isotope effect studies of these enzymes suggest the formation of ribosyl oxocarbenium transition states leading to and from the covalent intermediates. The combination of transition state analysis, transition state analogues, and structural approaches now provides the necessary tools to fully characterize the atomic steps in ribosyl transfer reaction coordinates.

ACKNOWLEDGMENT

The authors thank Prof. Robin Ferrier of Industrial Research Ltd. for critical reviews of the work.

REFERENCES

1. Schramm, V. L. (1998) *Annu. Rev. Biochem. 67*, 693−720.
2. Tao, W., Grubmeyer, C., and Blanchard, J. S. (1996) *Biochemistry 35*, 14−21.
3. Chen, X.-Y., Berti, P. J., and Schramm, V. L. (2000) *J. Am. Chem. Soc. 122*, 1609−1617.
4. Degano, M., Almo, S. C., Sacchettini, J. C., and Schramm, V. L. (1996) *Biochemistry 37*, 6277−6285.
5. Shi, W., Li, C. M., Tyler, P. C., Furneaux, R. H., Cahill, S. M., Girvin, M. E., Grubmeyer, C., Schramm, V. L., and Almo, S. C. (1999) *Biochemistry 38*, 9872−9880.
6. Shi, W., Li, C. M., Tyler, P. C., Furneaux, R. H., Grubmeyer, C., Schramm, V. L., and Almo, S. C. (1999) *Nat. Struct. Biol. 6*, 588−596.
7. Zechel, D. L., and Withers, S. G. (2000) *Acc. Chem. Res. 33*, 11−18.
8. Uitdehaag, J. C., Mosi, R., Kalk, K. H., van der Veen, B. A., Dijkhuizen, L., Withers, S. G., and Dijkstra, B. W. (1999) *Nat. Struct. Biol. 6*, 432−436.
9. Jencks, W. P. (1980) *Acc. Chem. Res. 13*, 161−169.
10. Carey, F. A., and Sundberg, R. J. (1990) in *Advanced Organic Chemistry, Part A: Structure and Mechanism*, 3rd ed., pp 261−270, Plenum Press, New York.
11. Parks, R. E., Jr., and Agarwal, R. B. (1972) *Enzymes, 3rd Ed. 7*, 483−514.
12. Bzowska, A., Kulikowska, E., and Shugar, D. (1990) *Z. Naturfosch. 45c*, 59−70.
13. Hershfield, M. S., and Mitchell, B. S. (1995) in *The Metabolic Basis of Inherited Disease* (Scriber, C. R., Beaudet, A. L., Sly, W. S.,and Valle, D., Eds.) 7th ed., Chapter 52, pp 1725−1768, McGraw-Hill, Inc., New York.
14. Miles, R. W., Tyler, P. C., Furneaux, R. H., Bagdassarian, C., and Schramm, V. L. (1998) *Biochemistry 37*, 8615−8621.
15. Kline, P. C., and Schramm, V. L. (1993) *Biochemistry 32*, 13212−13219.
16. Evans, G. B., Furneaux, R. H., Gainsford, G. J., Schramm, V. L., and Tyler, P. C. (2000) *Tetrahedron 56*, 3053−3062.
17. Mao, C., Cook, W. J., Zhou, M., Federov, A. A., Almo, S. C., and Ealick, S. E. (1998) *Biochemistry 37*, 7135−7146.
18. Wang, F., Miles, R. W., Kicska, G., Nieves, E., Schramm, V. L., and Angeletti, R. H. (2000) *Protein Sci. 9*, 1660−1668.
19. Gelbin, A., Schneider, B., Clowney, L., Hsieh, S.-H., Olson, W. K., and Berman, H. M. (1996) *J. Am. Chem. Soc. 118*, 519−529.
20. Horenstein, B. A., Parkin, D. W., Estupinan, B., and Schramm, V. L. (1991) *Biochemistry 30*, 10788−10795.
21. Lin, J., and Frey, P. A. (2000) *J. Am. Chem. Soc. 122*, 11258−11259.
22. Erion, M. D., Takabayashi, K., Smith, H. B., Kessi, J., Wagner, S., Honger, S., Shames, S. L., and Ealick, S. E. (1997) *Biochemistry 36*, 11725−11748.
23. Erion, M. D., Stoeckler, J. D., Guida, W. C., Walter, R. L., and Ealick, S. E. (1997) *Biochemistry 36*, 11735−11748.
24. Amyes, T. L., and Jencks, W. P. (1989) *J. Am. Chem. Soc., 111*, 7888−7900.
25. Kline, P. C., and Schramm, V. L. (1992) *Biochemistry 31*, 5964−5973.
26. Heroux, A., White, E. L., Ross, L. J., Davis, R. L., and Borhani, D. W. (1999) *Biochemistry 38*, 14495−14506.
27. Sauve, A. A., Deng, H., Angeletti, R. H., and Schramm, V. L. (2000) *J. Am. Chem. Soc. 122*, 7855−7859.
28. Porter, D. J., Merrill, B. M., and Short, S. A. (1995) *J. Biol. Chem. 279*, 15551−15556.
29. Otwinowski, Z., and Minor, W. (1997) *Methods Enzymol. 276*, 307−326.
30. Osborne, W. R. (1980) *J. Biol. Chem. 255*, 7089−7092.
31. Brunger, A. T. (1992) *X-PLOR Manual, Version 3.1*, Yale University Press, New Haven, CT.
32. Brunger, A. T. (1992) *Nature 355*, 472−475.
33. Laskowski, R. A., MacArthur, M. W., Moss, D. S., and Thornton, J. (1993) *J. Appl. Crystallogr. 26*, 283−291.
34. Evan, S. V. (1993) *J. Mol. Graphics 11*, 134−138.

BI002499F